Available online at www.sciencedirect.com
ScienceDirect
Trans. Nonferrous Met. Soc. China 34(2024) 3042−3053
Transactions of Nonferrous Metals Society of China
www.tnmsc.cn

Efficient removal of Al(III) and P507 from high concentration $MgCl_2$ solution based on in-situ reaction strategy

Qiang WANG[1,2,3], Meng WANG[1,3], Zong-yu FENG[1,3], Yong-qi ZHANG[1,3], Xiao-wei HUANG[1,2,3,4], Xiang-xin XUE[2]

1. National Engineering Research Center for Rare Earth, GRIREM Advanced Materials Co., Ltd., Beijing 100088, China;
2. School of Metallurgy, Northeastern University, Shenyang 110819, China;
3. General Research Institute for Nonferrous Metals, Beijing 100088, China;
4. GRIMAT Engineering Institute Co., Ltd., Beijing 101407, China

Received 16 April 2023; accepted 17 August 2023

Abstract: For a highly efficient recycling of a wastewater containing a high concentration of $MgCl_2$, Al(III) and P507 were scheduled to be removed in advance. In this study, the in-situ removal of Al(III) and P507 from a high concentration $MgCl_2$ solution at different pH values and Al/P molar ratios was investigated. The results showed that P507 formed organic complexes of $Al_x(OH)_y^{z+}$-P507 at pH of 2.0−4.0. At pH of 4.0−5.0, Al(III) precipitated and transferred into $Al(OH)_3$ with a flocculent amorphous morphology. Active sites on the $Al(OH)_3$ surface enhanced the removal efficiency of P507. At pH of 6.0−6.5, Al(III) and Mg(II) formed layered crystalline $Al(OH)_3$ and $MgAl_2(OH)_8$ with small pore channels and fewer active sites, resulting in a reduced removal efficiency of P507. When the Al/P molar ratio exceeded 13 and the pH was between 4.0 and 5.0, the removal rates of both Al(III) and P507 were higher than 98%, while the concentration loss of Mg(II) was only 0.2%−0.9%.

Key words: in-situ removal; Al(III); P507; $MgCl_2$ solution; pH; Al/P molar ratio

1 Introduction

Solvent extraction is the most common method for the separation and purification of rare earths. 2-ethylhexyl phosphate mono-2-ethylhexyl ester (P507) is one of the commonly used acidic organic extractants for the separation and purification of mixed chlorinated rare earth solutions [1]. It should be pre-saponified to balance the extraction equilibrium acidity of the aqueous phase in rare earth separation and purification. When traditional agents, ammonia and liquid alkali, are used for the saponification of P507, a wastewater containing high concentration of NH_4Cl and NaCl is generated, which is costly and difficult to be treated [2]. To solve the above problems, a series of methods were proposed by FENG et al [3]. MgO or $Mg(HCO_3)_2$ were used to replace ammonia and liquid alkali for the extraction and separation of rare earths. Thus, the NH_4Cl and NaCl wastewater was avoided. However, the $MgCl_2$ wastewater was generated in the new processes. For the reutilization of the useful components in the $MgCl_2$ wastewater, a spray pyrolysis−acid−base recycling technology was applied by FENG et al [4] to treat the $MgCl_2$ wastewater. Products of MgO and HCl were obtained and returned to the separation and purification process. This study aims to develop a pretreatment process of $MgCl_2$ wastewater for the

Corresponding author: Meng WANG, Tel: +86-13401082686, E-mail: warmmer69@163.com;
Xiao-wei HUANG, Tel: +86-13501282167, E-mail: hxw0129@126.com
DOI: 10.1016/S1003-6326(24)66594-5

removal of Al(III) and P507, which are adverse to the spray pyrolysis process and product quality.

Organic oils in a solution can be classified into four types: suspended, dispersed, emulsified, and dissolved. Suspended and dispersed oils can be removed from the solution by static oil separation and air flotation–ultrasonic emulsion breaking methods. Emulsified and dissolved oils can be removed by various methods, including coagulation and sedimentation, oxidation, and membrane filtration. However, the high costs of the methods and unsatisfactory performances of the agents limit their industrial applications [5−8]. Adsorption is regarded an effective method for removal of oil from wastewater [9]. YIN et al [10] added $Al_2(SO_4)_3$ and liquid alkali for the treatment of a low-concentration rare earth sulfate raffinate water. $Al(OH)_3$ was able to adsorb P507 to reduce its concentration to lower than 2 mg/L. LI et al [11] created a novel adsorbent, ORZ, for oil removal, which is stable in acids, bases, and organic solvents. It can remove organic matter selectively from solutions through physical adsorption and molecular screening. The concentration of oil can be reduced to lower than 5 mg/L. CAI et al [12] used $Al_2(SO_4)_3$ as a flocculant to treat a low-concentration rare earth sulfate raffinate. By controlling the pH of the solution, the removal rate of oil reached 85%.

The above studies focused on the removal of oil from low-concentration salt solutions by adsorption. The mechanism should be further explained. The removal of oil from a high-salt wastewater has been rarely reported. In this study, the $MgCl_2$ concentration of the solution is high, 220 g/L. The efficient removal of impurities from a $MgCl_2$ solution with a high concentration without loss of Mg(II) is of significance for a comprehensive salt recovery and utilization ratio.

2 Experimental

2.1 Experimental materials

$MgCl_2·6H_2O$ and $AlCl_3·6H_2O$ were purchased from Xilong Chemical Co. Ltd. and Aladdin Reagent (Shanghai) Co., Ltd., respectively. NaOH was acquired from Beijing Chemical Factory. The above agents were analytically pure. P507 and kerosene were procured from Chongqing Kopper Chemical Industry Co., Ltd. Their purity was higher than 95%.

2.2 Experimental method

A relatively stable aqueous solution containing P507 was prepared using a powerful mixing. A 220 g/L $MgCl_2$ solution was prepared by adding $MgCl_2·6H_2O$. The corresponding mass of $AlCl_3·6H_2O$ was added to obtain solutions containing 100, 300, and 600 mg/L Al(III). The experiments were carried out at 298 K. The pH of the solutions was adjusted using 0.1 mol/L liquid alkali and hydrochloric acid. When the target pH was reached and stabilized, the supernatant and precipitate were collected after 24 h of standing and clarification for an analysis.

2.3 Analysis methods

The content of P507 in this study was expressed based on the content of P. P507 was converted to orthophosphate by adding nitric and perchloric acids. The P content in the solution was then measured. The removal rate of Al(III) and P507 was calculated as

$$\beta = (C_0 - C_e)/C_0 \times 100\% \quad (1)$$

where β is the removal rate, C_0 is the initial concentration of the substance in the solution, and C_e is the residual concentration of the substance in the solution after adsorption.

The concentration of each component of the solution was determined using inductively coupled plasma optical emission spectrometry (PerkinElmer Optima 8300, USA). The phase characterization was performed using X-ray diffractometry (XRD, Rigku, Japan) in a scanning range of 10°−90° using a Cu K_α radiation and a scanning speed of 4 (°)/min. The crystalline structure and elemental content were determined using transmission electron microscopy (TEM, Thermo Fisher Scientific Talos F200X, USA). The surface groups and binding energies of the elements were analyzed by Fourier-transform infrared (FTIR) spectroscopy (Nicolet Nexus 6700, China) and X-ray photoelectron spectroscopy (XPS, Thermo Scientific K-Alpha, USA), respectively. The surface electrical properties and particle size were characterized by a zeta potential meter (BeNano 90, Better, China). The morphology of the sample was observed by scanning electron microscopy (SEM, JSM−7610F Plus, Japan). The pore size was measured by a nitrogen adsorption–desorption instrument (Quadrasorb SI, Quantachrome, USA). The samples were dried in a vacuum at 378 K for 3 h before the measurement.

3 Results and discussion

3.1 Effect of pH on precipitation of Al(III)

According to a comprehensive analysis of K_{sp} (K_{sp} is the solubility product constant) and concentration of Al(III) in the solution, the precipitation pH of Al(III) was between 3.6 and 4.7 [13]. Thus, the experimental pH was set in a range of 4.0−6.5. To clarify the precipitation behavior of Al(III) at different pH values, the physical phase, composition, micromorphology, pore capacity, and pore size of aluminum-containing hydrates were investigated.

XRD patterns of the aluminum-containing hydrates with varying pH values are shown in Fig. 1. When pH was between 4.0 and 5.0, the patterns of the aluminum-containing hydrates exhibited broad peaks, which indicates their amorphous morphology. However, when the pH was increased to 6.0 and 6.5, the patterns exhibited characteristic peaks, indicating their crystalline structure. In summary, as the pH increased from 4.0 to 6.5, the aluminum-containing hydrates transformed from amorphous to crystalline. By comparing the obtained patterns to the standard PDF card, the phases of the aluminum-containing hydrates were identified to be $Al(OH)_3$ (PDF#09-0096) and $MgAl_2(OH)_8$ (PDF#35-1274).

Figure 2(a) shows TEM analysis results of the aluminum-containing hydrates at pH of 4.0. There are no lattice streaks in the high-resolution images and no diffraction rings or spots in the selected area electron diffraction pattern, which indicated that $Al(OH)_3$ was amorphous. Figure 2(b) shows TEM analysis results of the aluminum-containing hydrates at pH of 6.5, where lattice streaks were observed in the high-resolution images, and the diffraction rings were visible in the selected area electron diffraction pattern, which indicated that the aluminum-containing hydrates were crystalline. By analyzing and comparing the lattice spacings, the corresponding phases were identified to be $Al(OH)_3$ and $MgAl_2(OH)_8$. The results suggest that Mg(II) in the solution coprecipitated with Al(III). As MgAl-LDH (LDH represents layered double hydroxides) exhibits a typical lamellar crystal structure, the lamellar crystals of the aluminum-containing hydrates were attributed to the induced growth of MgAl-LDH [14].

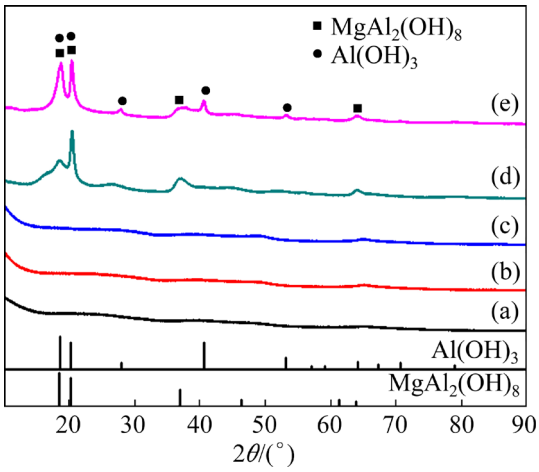

Fig. 1 XRD patterns of aluminum-containing hydrates at Al/P molar ratio of 13 and different pH values: (a) pH=4.0; (b) pH=4.5; (c) pH=5.0; (d) pH=6.0; (e) pH=6.5

The element analysis results in Figs. 2(a) and (b) reveal that the main elements of the aluminum-containing hydrates were aluminum and oxygen. Phosphorus and magnesium could also be observed. As the content of magnesium was low, only a small amount of Mg(II) coprecipitated with Al(III) and formed $MgAl_2(OH)_8$. The low content of phosphorus was attributed to the adsorption of P507 on the aluminum-containing hydrates. Furthermore, the phosphorus content of the aluminum-containing hydrates at pH of 4.0 was higher than that at pH of 6.5, which indicated that more P507 was adsorbed on the aluminum-containing hydrates at pH of 4.0. This was attributed to the numerous highly reactive under-coordinated atoms distributed on the surface of the poorly crystalline $Al(OH)_3$ providing adsorption sites for metal ions and organic acids to form inner or outer sphere complexes [15]. Hence, the amorphous $Al(OH)_3$ generated at pH of 4.0 exhibited a high adsorption capacity of P507.

To provide insights into the influence of the pH on the morphology of the aluminum-containing hydrates, the micromorphology and structure were characterized, as shown in Figs. 3−5 and Table 1. As shown in Fig. 3(a), the aluminum-containing hydrates were fluffy and flocculent at pH of 4.0. When pH increased to 5.0 and 6.5, the aluminum-containing hydrates transformed into fluffy, ribbon-like and lamellar structures, as shown in Figs. 3(b) and (c_1, c_2).

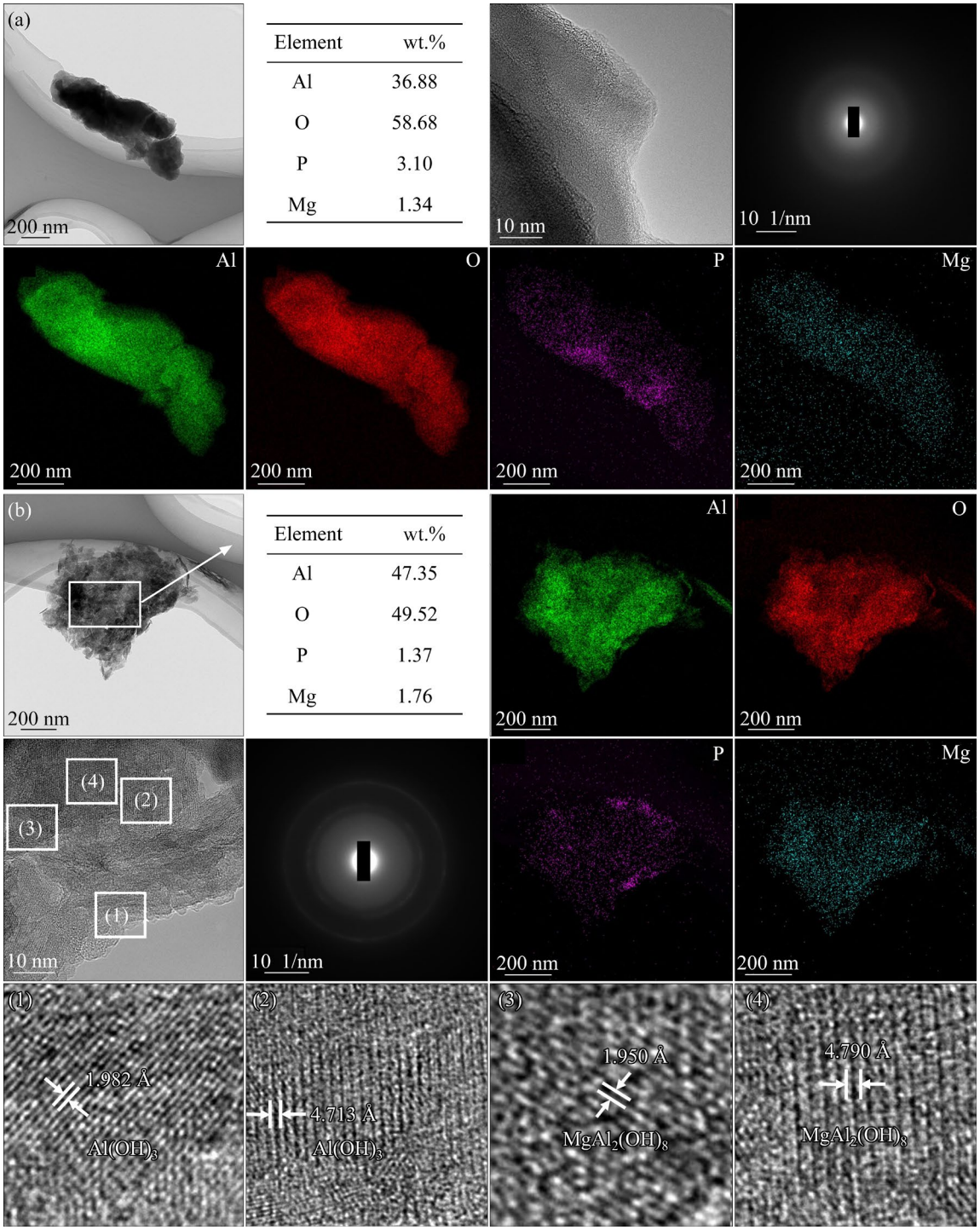

Fig. 2 TEM images of aluminum-containing hydrates at Al/P molar ratio of 13 and pH of 4.0 (a) and 6.5 (b)

The nitrogen adsorption and desorption curves were indicative of the pore shape of the aluminum-containing hydrates. As shown in Fig. 4, the pore shape of the aluminum-containing hydrates shifted from column-like to slit-like as the pH increased from 4.0 to 6.5 [16]. The column-like pore was attributed to the fluffy flocculent and fluffy ribbon-like structures, whereas the slit-like pore was attributed to the lamellar structures. Figure 5 shows that the pore size of the aluminum-containing hydrates was 1−100 nm.

Table 1 presents the average pore volume and pore diameter of the aluminum-containing hydrates. When the pH increased from 4.0 to 6.5, the pore volume increased from 0.01 to 0.376 cm^3/g, and the average pore diameter increased from 3.81 to

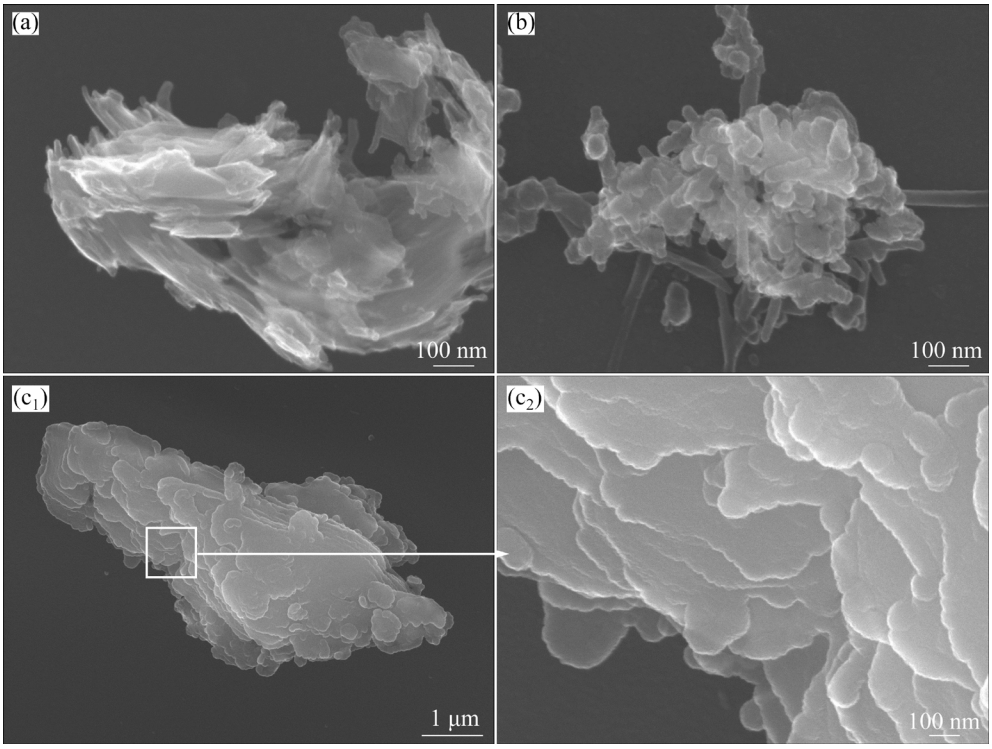

Fig. 3 Morphologies of aluminum-containing hydrates at Al/P molar ratio of 13 and pH of 4.0 (a), 5.0 (b) and 6.5 (c_1, c_2)

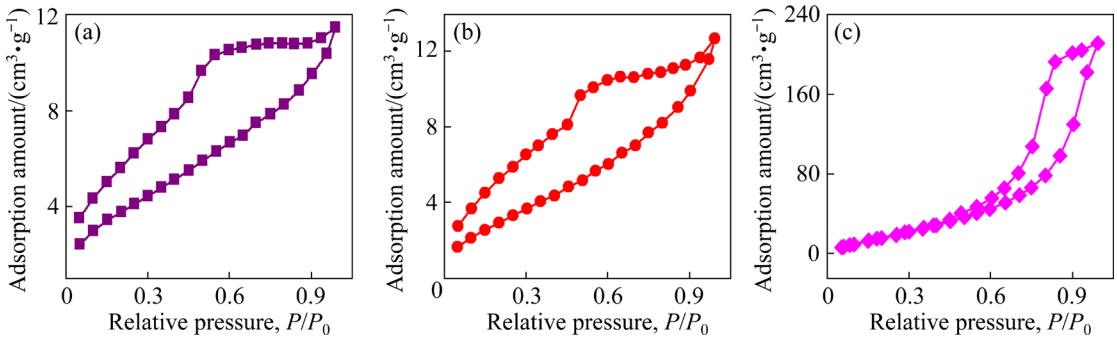

Fig. 4 Nitrogen adsorption and desorption curves of aluminum-containing hydrates at Al/P molar ratio of 13 and pH of 4.0 (a), 5.0 (b) and 6.5 (c)

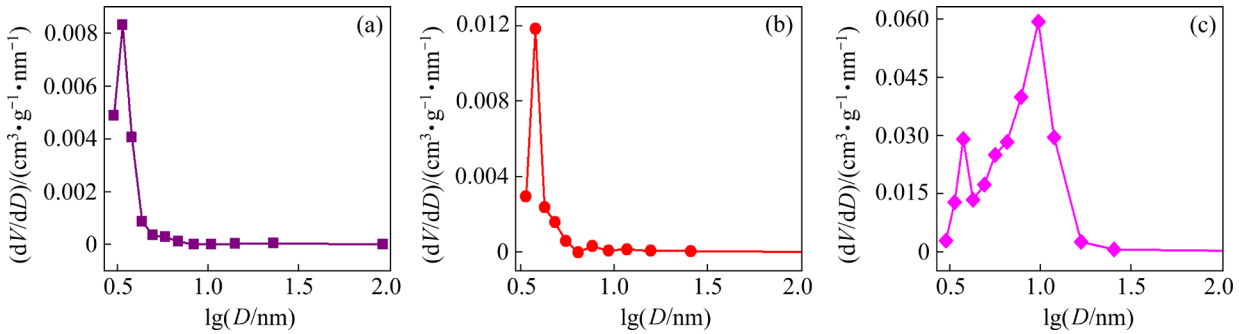

Fig. 5 Pore size (D) distribution curves of aluminum-containing hydrates at Al/P molar ratio of 13 and pH of 4.0 (a), 5.0 (b) and 6.5 (c)

9.71 nm. These observations indicated that the structure of the aluminum-containing hydrates underwent significant changes at different pH values. Based on the above analysis, pH had a significant influence on the morphology and structure of the aluminum-containing hydrates.

Table 1 Pore volume and average pore diameter of aluminum-containing hydrates at different pH values and Al/P molar ratio of 13

pH	Pore volume/($cm^3 \cdot g^{-1}$)	Average pore size/nm
4.0	0.01	3.81
5.0	0.013	3.82
6.5	0.376	9.71

3.2 Effect of Al/P molar ratio on removal of P507

Figure 6 shows the removal rates of Al(III) and P507, and retention rate of Mg(II) at different pH values and Al/P molar ratios. As shown in Fig. 6(a), the removal rate of Al(III) is almost unchanged with the increase in Al/P molar ratio. Thus, the Al/P molar ratio had a small effect on the Al(III) removal. The removal rate of Al(III) exceeded 98% when the pH was higher than 4.0. As shown in Fig. 6(b), in the investigated pH range, the removal rate of P507 at an Al/P molar ratio of 4 was lower than those at Al/P molar ratios of 13 and 26. Thus, the Al/P molar ratio had a significant effect on the removal of P507. Notably, the removal rate of P507 at an Al/P molar ratio of 13 was similar to that at 26, which suggests that the content of the aluminum-containing hydrates generated at an Al/P molar ratio of 4 was insufficient for P507 removal. Therefore, a suitable Al/P molar ratio is required for the effective removal of P507.

Figure 6(c) shows that the retention rate of Mg(II) is almost unchanged with the increase in Al/P molar ratio. However, the pH had a larger effect on the retention rate of Mg(II) than the Al/P molar ratio. At a higher pH, the coprecipitation of Mg(II) resulted in a loss of Mg(II). A higher Al(III) concentration in the solution resulted in a larger loss of Mg(II). Therefore, it is crucial to control the pH for the removal of Al(III) and P507. In summary, when the pH was in the range of 4.0−5.0 and the Al/P molar ratio was larger than 13, the removal rates of Al(III) and P507 exceeded 98%, which indicated that a deep removal of Al(III) and P507 could be achieved. The concentration loss of Mg(II) was only 0.2%−0.9%.

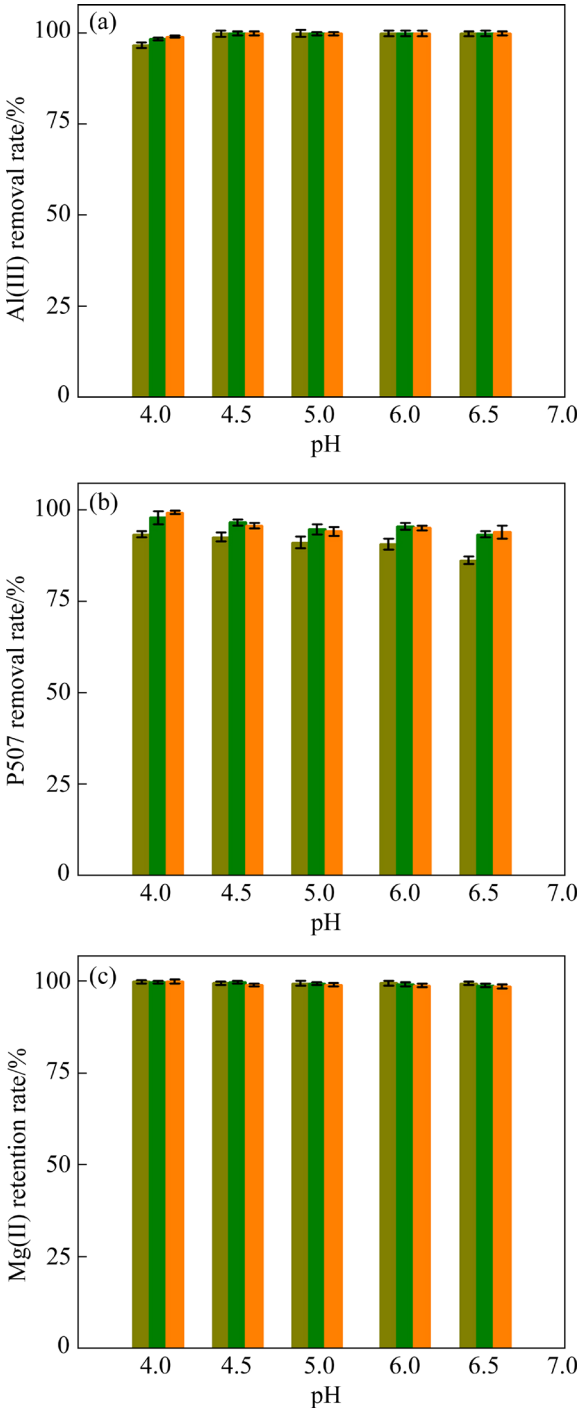

Fig. 6 Removal rates of Al(III) (a) and P507 (b), and retention rate of Mg(II) (c) at different pH values and Al/P molar ratios (dark yellow represents Al/P molar ratio of 4, olive represents Al/P molar ratio of 13, and orange represents Al/P molar ratio of 26)

3.3 Mechanism of P507 adsorption by aluminum-containing hydrates

To clarify the mechanism of the P507 adsorption by aluminum-containing hydrates, the particle size and zeta potential for both aluminum-containing hydrates and P507 in the solution were measured. As shown in Fig. 7(a), P507 oil droplets in the solution had a particle size of approximately 3.4 μm, considerably larger than the pore size of the aluminum-containing hydrates (1−100 nm). P507

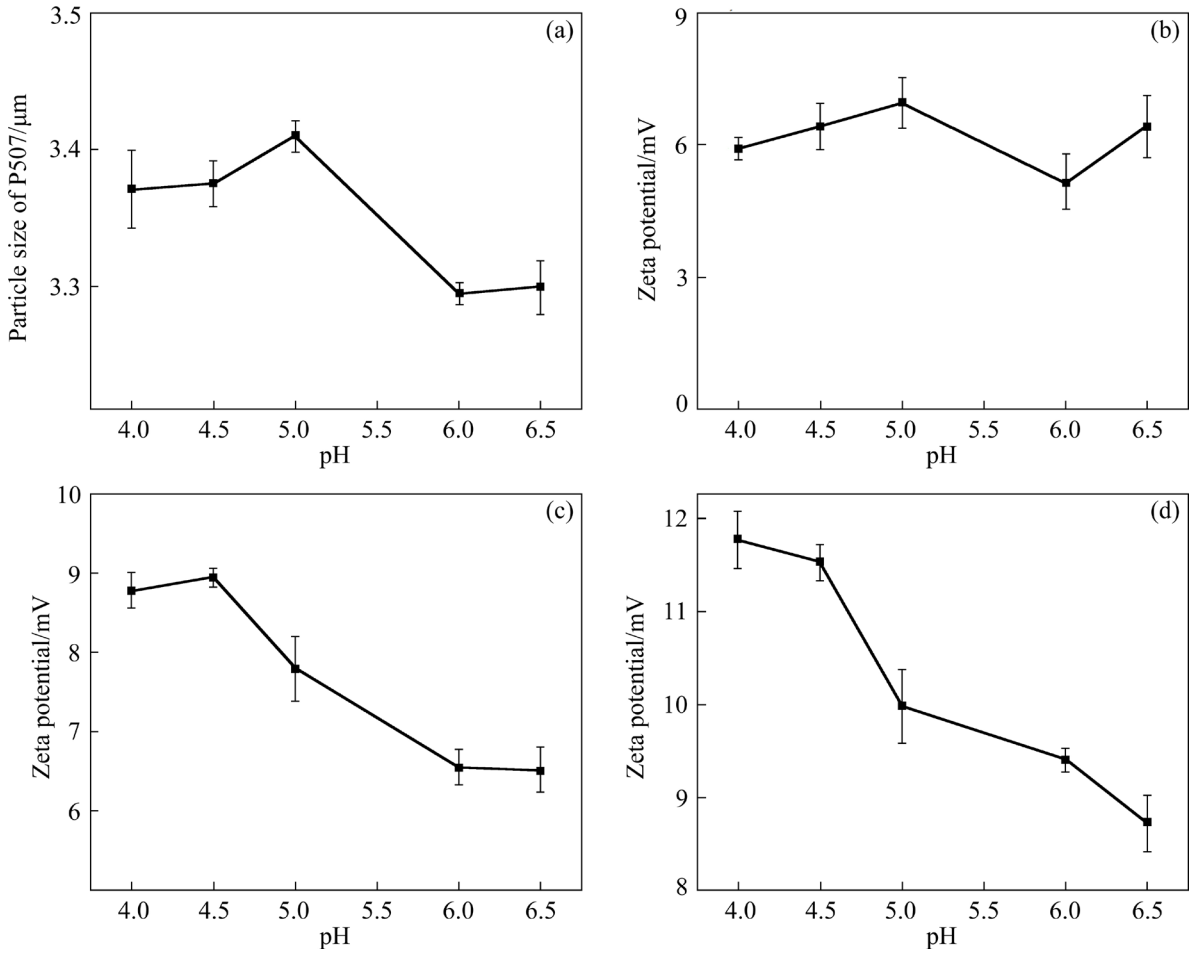

Fig. 7 Characterization of particle size and zeta potential: (a) Particle size of P507 oil droplets; (b) Zeta potential of P507 oil droplets; (c) Zeta potential of aluminum-containing hydrates before P507 adsorption; (d) Zeta potential of aluminum-containing hydrates after P507 adsorption

oil droplets could hardly penetrate the aluminum-containing hydrate pore channels. Thus, the in-situ removal of P507 was attributed to the adsorption of P507 on the outer surface of the aluminum-containing hydrates. More active sites could be observed on the aluminum-containing hydrates with the fluffy flocculent morphology than on those with the regular lamellar morphology. Thus, the aluminum-containing hydrates, generated at pH of 4.0, were more effective for the removal of P507.

Figures 7(b−d) show the zeta potentials of P507 oil droplets and aluminum-containing hydrate suspension before and after P507 adsorption at different pH values. The zeta potentials of both P507 oil droplets and aluminum-containing hydrates were positive, which indicated that the electrostatic forces were not the driving forces for P507 adsorption. After the P507 adsorption, the zeta potential of the aluminum-containing hydrates shifted to more positive values, which was attributed to the positive charge of the P507 oil droplets. In Fig. 7(d), the positive charge on the surface of the aluminum-containing hydrates decreased as the pH increased from 4.0 to 6.5.

To further analyze the adsorption behavior of P507, FTIR spectroscopy measurement was performed on the aluminum-containing hydrates after P507 adsorption at pH of 4.0, 5.0, and 6.5. FTIR spectra of pure $Mg(OH)_2$ and $Al(OH)_3$ and 1.5 mol/L P507 were also measured. The results are shown in Fig. 8. In Fig. 8(f), the peaks at 3700 and 1490 cm^{-1} are attributed to the hydroxyl stretching vibrations of $Mg(OH)_2$ [17,18]. As these peaks were not observed in the FTIR spectra of the aluminum-containing hydrates shown in Figs. 8(a−c), $Mg(OH)_2$ was not generated during the precipitation of Al(III).

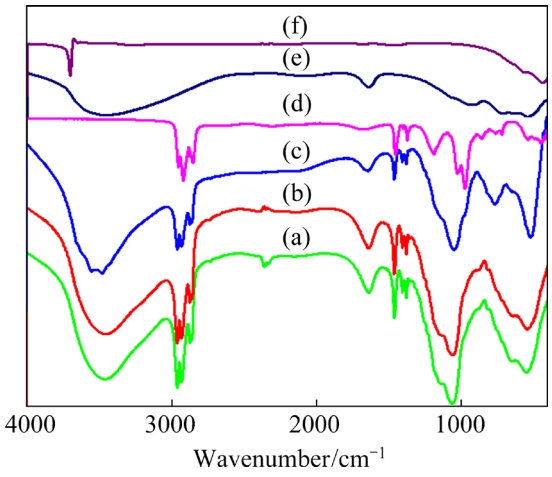

Fig. 8 FTIR spectra of aluminum-containing hydrates at Al/P molar ratio of 13 and pH of 4.0 (a), 5.0 (b), and 6.5 (c), and FTIR spectra of 1.5 mol/L P507 (d), $Al(OH)_3$ (e), and $Mg(OH)_2$ (f)

In Fig. 8(e), the broad peak at 3480 cm^{-1} is attributed to the stretching vibration of nonhydrogen-bonded terminal —OH groups, interlayer hydrogen-bonded —OH group, and side hydroxyl groups of $Al(OH)_3$ [19]. The peak at 1640 cm^{-1} is assigned to the bending vibrations of H—O—H in water [20]. The peak at 940 cm^{-1} is attributed to the hydroxyl deformation vibration of nonhydrogen-bonded Al—(OH)—Al groups [21,22]. The new vibrational characteristic peak at 760 cm^{-1} in Fig. 8(c) is attributed to the lattice vibration of the interlayer Mg(Al)—O, Mg(Al)—OH and O—Mg(Al)—O [23−25], which demonstrates the coprecipitation of Al(III) and Mg(II) at high pH values.

Figure 8(d) shows the FTIR spectrum of 1.5 mol/L P507. The characteristic peaks at 2960, 2930, 2870, 1460 and 1380 cm^{-1} are attributed to the antisymmetric stretching vibration of —CH_3 and —CH_2— [26,27]. Notably, these characteristic peaks could also be observed in the FTIR spectra of the aluminum-containing hydrates shown in Figs. 8(a−c), indicating the adsorption of P507 on the aluminum-containing hydrates. The peaks at 1030 and 980 cm^{-1} were vibrational characteristic peaks of P—C and P—O, respectively [28,29]. Furthermore, the characteristic peak at 1190 cm^{-1} weakened and blue-shifted with the increase in the pH, which indicated that P═O was involved in the coordination. As the characteristic peak at 1030 cm^{-1} was almost unchanged, P—C was not involved in the reaction. On the other hand, as the characteristic peak at 980 cm^{-1} disappeared, P—O was involved in the reaction. These findings suggested that P507 underwent a chemical reaction during the adsorption and removal. As the pH increased from 2.0 to 4.0, Al(III) was transferred to polynuclear hydroxy complexes by hydrolysis and the polymerization of the condensation reactions [30,31]. These complexes, including $Al_3(OH)_5^{4+}$, $Al_6(OH)_5^{3+}$, $Al_8(OH)_{20}^{4+}$, $Al_9(OH)_{23}^{4+}$, $Al_{13}(OH)_{33}^{6+}$, $Al(H_2O)_6^{3+}$ and $Al_2(H_2O)_8^{4+}$, are denoted as $Al_x(OH)_y^{z+}$. $Al_x(OH)_y^{z+}$-P507 organic complexes formed by ion exchange between Na-P507 and polynuclear hydroxy-polymeric aluminum ions [32−34].

To confirm the chemical reactions that occurred during the adjustment of the solution pH, XPS measurement of the aluminum-containing hydrates and 1.5 mol/L P507 was carried out, and the results are shown in Fig. 9. Detailed data are presented in Table 2. In Fig. 9(d), the P 2p peaks with binding energies of 133.71, 134.86 and 136.44 eV were attributed to P—C, P—O and P═O, respectively. They decreased after P507 was adsorbed on the aluminum-containing hydrates. These changes reflected the changes in the chemical environment surrounding P. Thus, the chemical reaction was verified [35].

In summary, Al(III) formed aluminum-containing hydrates by adjusting the solution pH, which were then removed. The aluminum-containing hydrates exhibited different properties at different pH values. They exhibited different adsorption capacities for P507. Figure 10 illustrates the in-situ removal mechanism of Al(III) and P507. When the pH increased from 2.0 to 4.0, Al(III) transformed into a poly-aluminum polymer. Saponification of P507 occurred. As a result, the organic complex of $Al_x(OH)_y^{z+}$-P507 formed. When the pH was 4.0−5.0, the flocculent amorphous $Al(OH)_3$ was generated. The irregular shape and large amount of active sites of the amorphous $Al(OH)_3$ favored the adsorption of P507 oil droplets. A higher P507 removal efficiency was achieved. When the pH was 6.0−6.5, $Al(OH)_3$ and $MgAl_2(OH)_8$ formed, which exhibited regular lamellar structures and small pore channels. The reduced active sites resulted in a lower P507 removal efficiency.

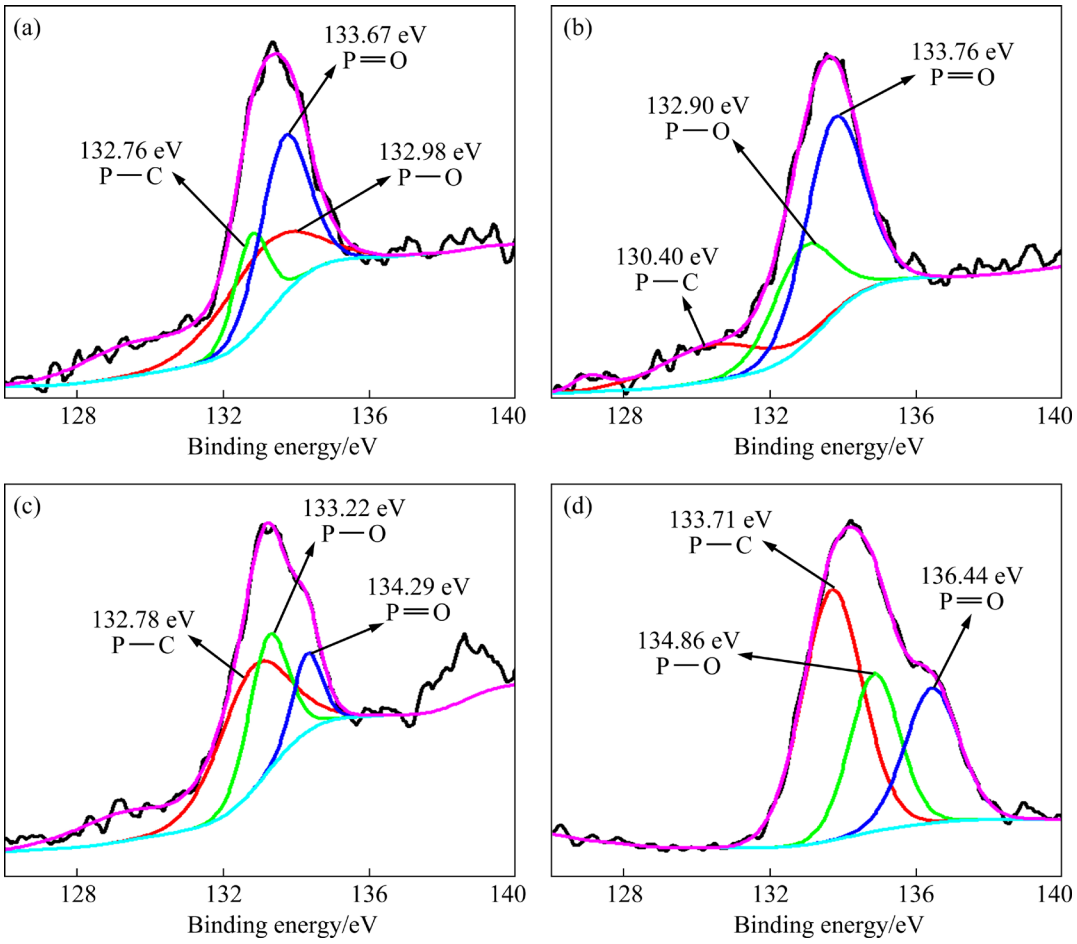

Fig. 9 Orbital binding energies of P 2p in aluminum-containing hydrates at Al/P molar ratio of 13 and pH of 4.0 (a), 5.0 (b) and 6.5 (c), and 1.5 mol/L P507 (d)

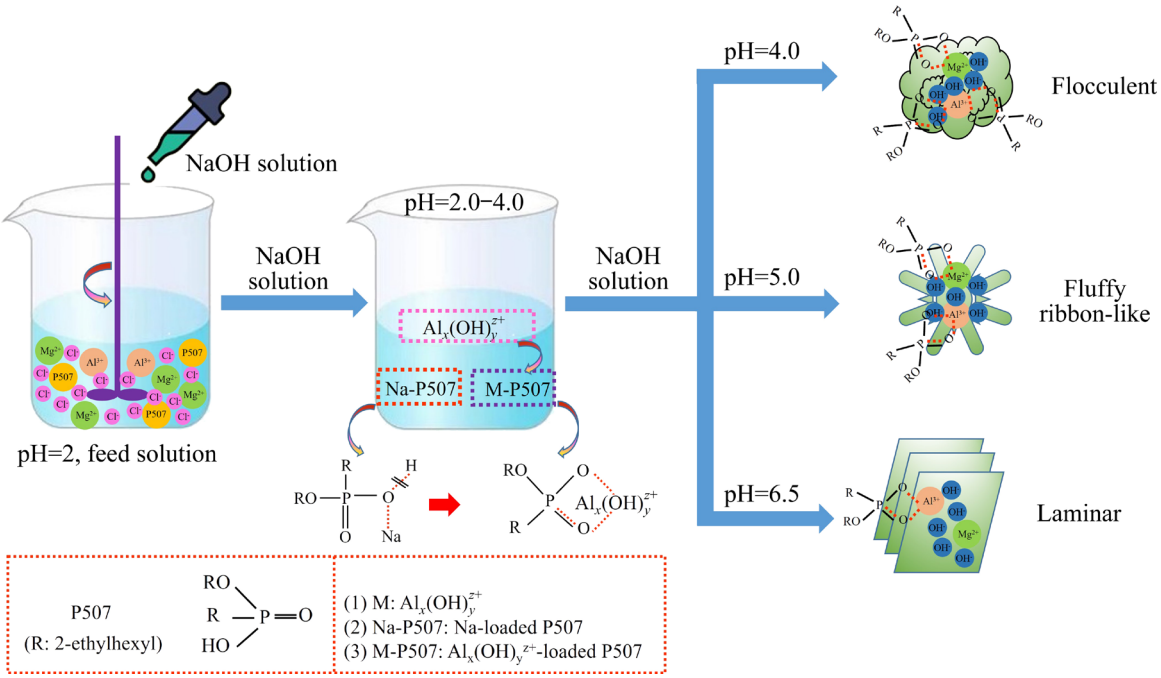

Fig. 10 Schematic diagram showing in-situ adsorption and impurity removal mechanism of Al(III) and P507

Table 2 P—C, P—O and P═O binding energies of aluminum-containing hydrates at different pH values and Al/P molar ratio of 13 and 1.5 mol/L P507

Content	Binding energy/eV		
	P—C	P—O	P═O
Aluminum-containing hydrate (pH = 4.0)	132.76	132.98	133.67
Aluminum-containing hydrate (pH = 5.0)	130.40	132.90	133.76
Aluminum-containing hydrate (pH = 6.5)	132.78	133.22	134.29
1.5 mol/L P507	133.71	134.86	136.44

4 Conclusions

(1) In the $MgCl_2$ solution with a high concentration, containing Al(III), the pH was adjusted by adding liquid alkali to achieve the in-situ precipitation of Al(III). The aluminum-containing hydrates were scheduled to be generated for the adsorption and removal of P507. The simultaneous removal of Al(III) and P507 was then achieved.

(2) When the pH was 2.0−4.0, Al(III) formed polynuclear hydroxyl complexes that exchanged ions with Na-P507 to form $Al_x(OH)_y^{z+}$-P507 organic complexes. When the pH was 4.0−5.0, the flocculent amorphous $Al(OH)_3$ with more active sites on the surface was generated, resulting in effective adsorption and removal of P507. When the pH was 6.0−6.5, a mixture of aluminum-containing hydrates, including crystalline $Al(OH)_3$ and $MgAl_2(OH)_8$, with a regular laminar structure and smaller pore channels, was generated. The reduced active sites resulted in a lower adsorption and removal efficiency of P507.

(3) At pH of 4.0−5.0 and Al/P molar ratio higher than 13, the deep removal of Al(III) and P507 could be achieved with a removal rate up to 98%. The concentration loss of Mg(II) was maintained below 0.9%.

CRediT authorship contribution statement

Qiang WANG: Conceptualization, Methodology, Software, Formal analysis, Investigation, Writing − Original draft, Visualization; **Meng WANG** and **Xiao-wei HUANG:** Conceptualization, Funding acquisition, Resources, Supervision, Writing − Review & editing; **Zong-yu FENG:** Visualization, Investigation; **Yong-qi ZHANG:** Software, Validation; **Xiang-xin XUE:** Resources, Supervision.

Declaration of competing interest

The authors declare that they have no known competing financial interests or personal relationships that could have appeared to influence the work reported in this paper.

Acknowledgments

The authors thank for the financial supports from the National Key Research and Development Program of China (No. 2022YFB3504501), the National Natural Science Foundation of China (Nos. 52274355, 91962211), and the Gansu Province Science and Technology Major Special Project, China (No. 22ZD6GD061).

References

[1] XIE Feng, ZHANG Ting-an, DREISINGER D, DOYLE F. A critical review on solvent extraction of rare earths from aqueous solutions [J]. Minerals Engineering, 2014, 56: 10−28.

[2] ZHANG Lin-nan, XU Bing-hui, GONG Ji-da, BU Tian-da. Membrane combination technic on treatment and reuse of high ammonia and salts wastewater in rare earth manufacture process [J]. Journal of Rare Earths, 2010, 28: 501−503.

[3] FENG Zong-yu, HUANG Xiao-wei, WANG Meng, ZHANG Guo-cheng. Progress and trend of green chemistry in extraction and separation of typical rare earth resources [J]. Chinese Journal of Rare Metals, 2017, 41(5): 604−611. (in Chinese)

[4] FENG Zong-yu, HUANG Xiao-wei, WANG Meng, SUN Xu, XIAO Chao, XU Yang, CHEN Shi-liang, PENG Xin-lin, ZHANG Yong-qi. A treatment method of rare earth smelting separation process containing magnesium and/or calcium waste liquid: CN patent, 111041249A [P]. 2018-10-11. (in Chinese)

[5] WU Peng, JIANG Lan-ying, HE Zhen, SONG Yang. Treatment of metallurgical industry wastewater for organic contaminant removal in China: Status, challenges, and perspectives [J]. Environmental Science: Water Research & Technology, 2017, 3(6): 1015−1031.

[6] XIAO Xin-jin, HUANG Jin, WANG Hui-juan, DENG Yang-wu. Research progress of deep removal oil in rare earth hydrometallurgy waste water [J]. Biological Chemical Engineering, 2021, 7(2): 146−150. (in Chinese)

[7] ZENG Biao, XIONG Chao, WANG Wei, LIN Guo, CHENG Song, CHANG Jun. Adsorption behavior and mechanism of Hg(II) on highly stable Zn-based metal organic frameworks [J]. Transactions of Nonferrous Metals Society of China, 2022, 32(10): 3420−3433.

[8] WANG Zhuo-jie, XU Long-hua, WU Hou-qin, ZHOU Huan, MENG Jin-ping, HUO Xiao-mei, HUANG Ling-yun.

Adsorption of octanohydroxamic acid at fluorite surface in presence of calcite species [J]. Transactions of Nonferrous Metals Society of China, 2021, 31(12): 3891−3904.

[9] RASHED M N. Adsorption technique for the removal of organic pollutants from water and wastewater [J]. Organic Pollutants: Monitoring, Risk and Treatment, 2013, 7: 167−194.

[10] YIN Wei-qiang, ZHAO Jin-hui, ZHAO Long-sheng, LIU De-peng, QI Shao-lei, FENG Zong-yu. Stability of emulsified oil droplets and demulsification mechanism of rare earth raffinate using Al^{3+} hydrolysis [J]. Chinese Journal of Rare Metals, 2022, 46(10): 1322−1330. (in Chinese)

[11] LI Zhi-qiang, TAO Li, LI Xu-ling, XIANG Bo, LIU Chen-ming, LIN Xiao. The component and deep removal technology of oil in rare earth extraction solutions [J]. Modern Chemical Research, 2020, 10: 1−4. (in Chinese)

[12] CAI Shui-dong, YANG Li-fen, SUN Yuan-yuan, LIU Yan-zhu, LI Yong-xiu. Organic phase lose in rare earth extraction by P507-kerosene and oil removal from raffinate phase by an aluminium sulphate coagulation method [J]. Chinese Rare Earths, 2017, 38(6): 33−40. (in Chinese)

[13] DONG Chun-xu, HE Gao-hong, ZHENG Wen-ji, BIAN Teng-fei, LI Mo, ZHANG Da-wei. Study on antibacterial mechanism of $Mg(OH)_2$ nanoparticles [J]. Materials Letters, 2014, 134: 286−289.

[14] PELIGRO F R, PAVLOVIC I, ROJAS R, BARRIGA C. Removal of heavy metals from simulated wastewater by in situ formation of layered double hydroxides [J]. Chemical Engineering Journal, 2016, 306: 1035−1040.

[15] HUANG P M, WANG M K, KAMPF N, SCHULZE D G. Aluminum hydroxides [J]. Soil Mineralogy with Environmental Applications, 2002, 7: 261−289.

[16] LIU Xiang-jun, XIONG Jian, LIANG Li-xi. Investigation of pore structure and fractal characteristics of organic-rich Yanchang formation shale in Central China by nitrogen adsorption/desorption analysis [J]. Journal of Natural Gas Science and Engineering, 2015, 22: 62−72.

[17] CHANG Lin-rong, CAO Fa-he, CAI Jing-shun, LIU Wen-juan, ZHANG Jiang-qing, CAO Chu-nan. Formation and transformation of $Mg(OH)_2$ in anodic coating using FTIR mapping [J]. Electrochemistry Communications, 2009, 11: 2245−2248.

[18] DONG Chun-xu, HE Gao-hong, LI Hao, ZHAO Rui, HAN Yue, DENG Yu-lin. Antifouling enhancement of poly(vinylidene fluoride) microfiltration membrane by adding $Mg(OH)_2$ nanoparticles [J]. Journal of Membrane Science, 2012, 387: 40−47.

[19] EGOROVA S R, LAMBEROV A A. Formation and distribution of phases during the dehydration of large hydrargillite floccules [J]. Inorganic Materials, 2015, 51(4): 331−389.

[20] LIANG Xue-feng, HOU Wan-guo, XU Ying-ming, SUN Guo-hong, WANG Lin, SUN Yang, QIN Xu. Sorption of lead ion by layered double hydroxide intercalated with diethylenetriaminepentaacetic acid [J]. Colloids and Surfaces A: Physicochemical and Engineering Aspects, 2010, 366: 50−57.

[21] FROST R L. Hydroxyl deformation in kaolins [J]. Clays and Clay Minerals, 1998, 46(3): 280−289.

[22] RUAN H D, FROST R L, KLOPROGGE J T. Comparison of Raman spectra in characterizing gibbsite, bayerite, diaspore and boehmite [J]. Journal of Raman Spectroscopy, 2001, 32(9): 745−750.

[23] LEE S Y, CHOI J W, SONG K G, CHOI K, LEE Y J, JUNG K W. Adsorption and mechanistic study for phosphate removal by rice husk-derived biochar functionalized with Mg/Al-calcined layered double hydroxides via co-pyrolysis [J]. Composites Part B: Engineering, 2019, 176: 107209.

[24] ZHANG Feng-rong, DU Na, SONG Shue, HOU Wan-guo. Mechano-hydrothermal synthesis of SDS intercalated LDH nanohybrids and their removal efficiency for 2,4-dichlorophenoxyacetic acid from aqueous solution [J]. Materials Chemistry and Physics, 2015, 152: 95−103.

[25] JUNG K W, LEE S Y, CHOI J W, HWANG M J, SHIM W G. Synthesis of Mg−Al layered double hydroxides-functionalized hydrochar composite via an in situ one-pot hydrothermal method for arsenate and phosphate removal: structural characterization and adsorption performance [J]. Chemical Engineering Journal, 2021, 420: 129775.

[26] IQBAL M, SAEED A, ZAFAR S I. FTIR spectrophotometry, kinetics and adsorption isotherms modeling, ion exchange, and EDX analysis for understanding the mechanism of Cd^{2+} and Pb^{2+} removal by mango peel waste [J]. Journal of Hazardous Materials, 2009, 164(1): 161−171.

[27] ZHU H Y, RICHES J D, BARRY J C. γ-alumina nanofibers prepared from aluminum hydrate with poly (ethylene oxide) surfactant [J]. Chemistry of Materials, 2002, 14(5): 2086−2093.

[28] GYPSER S, HIRSCH F, SCHLEICHER A M, FREESE D. Impact of crystalline and amorphous iron and aluminum hydroxides on mechanisms of phosphate adsorption and desorption [J]. Journal of Environmental Sciences, 2018, 70: 175−189.

[29] LIU Chuan-ying, CHEN Li, CHEN Ji, ZOU Dan, DENG Yue-feng, LI De-qian. Application of P507 and isooctanol extraction system in recovery of scandium from simulated red mud leach solution [J]. Journal of Rare Earths, 2019, 37: 1002−1008.

[30] BROSSET C, BIEDERMANN G, SILLEN L G. Studies on the hydrolysis of metals ions [J]. Acta Chemica Scandinavica, 1954, 8(10): 1917−1926.

[31] TRAWCZYNSKI J T. Effect of aluminum hydroxide precipitation conditions on the alumina surface acidity [J]. Industrial & Engineering Chemistry Research, 1996, 35(1): 241−244.

[32] CHEN K H, HE Y, SRINIVASAKANNAN C, LI S W, YIN S H, PENG J H, GUO S H, ZHANG L B. Characterization of the interaction of rare earth elements with P507 in a microfluidic extraction system using spectroscopic analysis [J]. Chemical Engineering Journal, 2019, 356: 453−460.

[33] WU Wen-yuan, LI Dong, ZHAO Zhi-hua, CHEN Jian-li, ZHANG Feng-yun, YIN Shao-hua, QIAN Mei-li, BIAN Xue. Formation mechanism of micro emulsion on aluminum and lanthanum extraction in P507-HCl system [J]. Journal of Rare Earths, 2010, 28: 174−178.

[34] ZENG Xian-jie, XU Li, DENG Tao, ZHANG Cheng-yi, XU Wei, ZHANG Wen. Polymer inclusion membranes with P507-TBP carriers for lithium extraction from brines [J].

Membranes, 2022, 12(9): 839.
[35] WU Dong-bei, SUN Yan-hong, WANG Qiang. Adsorption of lanthanum(III) from aqueous solution using 2-ethylhexyl phosphonic acid mono-2-ethylhexyl ester-grafted magnetic silica nanocomposites [J]. Journal of Hazardous Materials, 2013, 260: 409−419.

基于原位反应策略高效去除高浓度 $MgCl_2$ 溶液中的 Al(III)和 P507

王 强[1,2,3]，王 猛[1,3]，冯宗玉[1,3]，张永奇[1,3]，黄小卫[1,2,3,4]，薛向欣[2]

1. 有研稀土新材料股份有限公司 稀土国家工程研究中心，北京 100088；
2. 东北大学 冶金学院，沈阳 110819；
3. 北京有色金属研究总院，北京 100088；
4. 有研工程技术研究院有限公司，北京 101407

摘 要：为了实现含高浓度 $MgCl_2$ 废水的循环利用，需要提前去除其中的 Al(III)和 P507。本文作者研究了不同 pH 值以及不同 Al/P 摩尔比对 Al(III)和 P507 原位去除效果的影响。研究结果表明，当 pH 值为 2.0~4.0 时，P507 会形成 $Al_x(OH)_y^{z+}$-P507 有机配合物；当 pH 值为 4.0~5.0 时，Al(III)沉淀为具有较多表面活性位点的絮状非晶 $Al(OH)_3$，使得 P507 的吸附去除效果较好；当 pH 值为 6.0~6.5 时，Al(III)和 Mg(II)形成层状晶体 $Al(OH)_3$ 和 $MgAl_2(OH)_8$，表面活性位点较少，使得 P507 吸附去除效果变差。此外，当 Al/P 摩尔比大于 13、pH 值为 4.0~5.0 时，Al(III)和 P507 的去除率皆可达到 98%以上，同时 Mg(II)的浓度损失仅为 0.2%~0.9%。

关键词：原位除杂；Al(III)；P507；$MgCl_2$ 溶液；pH；Al/P 摩尔比

(Edited by Wei-ping CHEN)